Reductions of *Grin2a* in adolescent dopamine neurons confers aberrant salience and related psychosis phenotype

Michelle L. Kielhold[1], David S. Jacobs[1], Alejandro Torrado-Pacheco[1], Joseph J. Lebowitz[2], Angela J. Langdon[3], John T. Williams[2], Larry S. Zweifel[4], and Bita Moghaddam[1]

[1]Department of Behavioral Neuroscience [2]Vollum Institute, Oregon Health & Science University, Portland, Oregon

[3]Intramural Research Program, National Institute of Mental Health, National Institutes of Health, Bethesda, MD

[4]Department of Pharmacology, University of Washington, Seattle, Washington

Corresponding author: Bita Moghaddam bita@ohsu.edu

Abstract

Psychosis is a hallmark of schizophrenia. It typically emerges in late adolescence and is associated with dopamine abnormalities and aberrant salience. Most genes associated with schizophrenia risk involve ubiquitous targets that may not explain delayed emergence of dopaminergic disruptions. This includes *GRIN2A,* the gene encoding the GluN2A subunit of the NMDA receptor. Both common and rare variants of *GRIN2A* are considered genetic risk factors for schizophrenia diagnosis. We find that *Grin2a* knockout in dopamine neurons during adolescence is sufficient to produce a behavioral phenotype that mirrors aspects of psychosis. These include disruptions in effort optimization, salience attribution, and ability to utilize feedback to guide behavior. We also find a selective effect of this manipulation on dopamine release during prediction error signaling. These data provide mechanistic insight into how variants of *GRIN2A* may lead to the latent presentation of aberrant salience and abnormalities in dopamine dynamics. This etiologically relevant model may aid future discovery of course altering treatments for schizophrenia.

Introduction

Schizophrenia (SCZ) is a common [1] and devastating mental health disorder. Despite the profound social, economic, and personal costs associated with this illness, its complex nature has stymied the development of treatments that may prevent or alter the course of the disorder. The etiological complexity of SCZ can be attributed primarily to two characteristics of the disorder. First, SCZ symptoms are categorically different, involving distinct constructs and temporal patterns of onset. Cognitive and affective symptoms typically manifest in childhood whereas the onset of psychosis, the so-called positive symptoms, is often observed in late adolescence. Second, while SCZ is highly heritable [2-5], genetic contributions to this disorder have not been easy to decipher. Recently, however, several highly powered genome wide association studies (GWAS) and rare coding variant studies have advanced the field by identifying multiple SCZ risk genes. One of the strongest genetic candidates is *GRIN2A*, which encodes the GluN2A subunit of the NMDA receptor [6-13]. Both common variants and rare missense and protein-truncating variants of *GRIN2A* were identified as genetic risk factors for schizophrenia. Consistent with this discovery, *Grin2a* mutant mice display a wide range of aberrant cortical and motor activity [12-14].

Discovery of *GRIN2A* involvement has generated a great deal of enthusiasm in the field because it may explain the distinct temporal pattern of symptom expression in SCZ. Both human and rodent data have established a positive association between early neurodevelopment and *GRIN2A/Grin2a* expression in the brain [15-19]. Specifically, expression in cortical and hippocampal regions steeply increases with age, beginning perinatally (humans) or after birth (rodents). Detrimental effects of a reduction in functional *GRIN2A* would, therefore, emerge during this early developmental stage, consistent with the timeline of cognitive and affective symptom expression in SCZ. But why would psychosis remain latent until late adolescence or early adulthood? This is the question we sought to answer in the current study by investigating the role of *Grin2a* specifically within the dopaminergic system. This is because, unlike cognitive or negative symptoms, these late-emerging positive symptoms can be alleviated with dopamine receptor antagonists [20-24] and are associated with abnormalities in striatal dopamine neurotransmission [25-30].

Here, we designed an etiologically relevant rodent model to gain mechanistic insight into how reduced function of *GRIN2A* can lead to latent presentation of psychosis and dopaminergic abnormalities. We found that, unlike cortical regions where GluN2A remains stable during adolescence, levels in dopamine neuron-containing regions decline at this age. This suggested that a loss of function in *Grin2a* may exaggerate this natural decline and be most detrimental to dopamine neurotransmission during adolescence, thus contributing to the emergence of psychosis at or after this time. To investigate this potential link between *Grin2a* loss of function and post-adolescent expression of psychosis, we selectively manipulated *Grin2a* in adolescent dopamine neurons. This

developmental manipulation was sufficient to cause selective behavioral changes relevant to psychosis including abnormal salience attribution and disrupted dopamine release during prediction error signaling.

RESULTS

Adolescent expression of GluN2A and selective reduction of GluN2A in adolescent dopamine neurons

In rodents, cortical regions including prefrontal cortex and the hippocampus, do not express GluN2A at birth, but levels rapidly increase postnatally, reaching adult levels around weaning [18,19,31]. It is, however, not known if GluN2A levels remain stable between weaning and adulthood. We quantified GluN2A levels in male and female rats immediately after weaning (P21), during adolescence (P35, P45), and adulthood (P80) in the prefrontal cortex (PFC), hippocampus, ventral tegmental area (VTA), and substantia nigra (SN) (Figure 1A, S1). We found GluN2A levels in the PFC and hippocampus remained stable between ages P21 and P80 (Figure 1B). In contrast, GluN2A levels were labile in dopamine neuron-rich regions during adolescence. In both the VTA and SN, there was loss of GluN2A after P21, declining to adult levels in mid-late adolescence (Figure 1C). We hypothesized that the damaging variants of *GRIN2A* implicated in SCZ, may augment this natural reduction during adolescence, providing a mechanism for the emergence of psychosis at this developmental stage (Figure 1D). We tested this idea by establishing a model of adolescent dopamine neuron-selective knockout of *Grin2a* (DA-*Grin2a* KO) by infusing a Cre-inducible CRISPR/Cas9 virus targeting *Grin2a* into the VTA of TH::Cre rats. This virus was co-infused with a Cre-dependent virus that would express green fluorescent protein (GFP) (Figure 1E). Viral infusions were performed after weaning (P21) and expression was assessed following a 2-week incubation period. Immunohistochemistry confirmed cell-specific virus expression. Staining for the hemagglutinin (HA)-tag on the DA-*Grin2a* KO virus significantly overlapped with GFP (Figure 1F) and this expression was specific to dopamine neurons as there was significant co-expression of GFP and tyrosine hydroxylase (TH) (Figure 1G). Functional reduction of GluN2A in GFP+ neurons was established with recordings in slice preparation (Figure 1H). Bath application of a GluN2A-specific antagonist (TCN201) resulted in a reduction of the glutamate-induced current in controls whereas DA-*Grin2a* KO cells showed a significantly blunted response to the drug (Figure 1I). This reduction was specific to GluN2A-containing NMDA receptors as a GluN2B-targeting antagonist (ifenprodil) produced similar effects in cells of both control and DA-*Grin2a* KO animals (Figure 1J). Finally, the extent of this regional loss of GluN2A was determined through Western blot analysis. We observed an approximate 50% reduction of GluN2A in the VTA of DA-*Grin2a* KO animals compared to controls (Figure 1K).

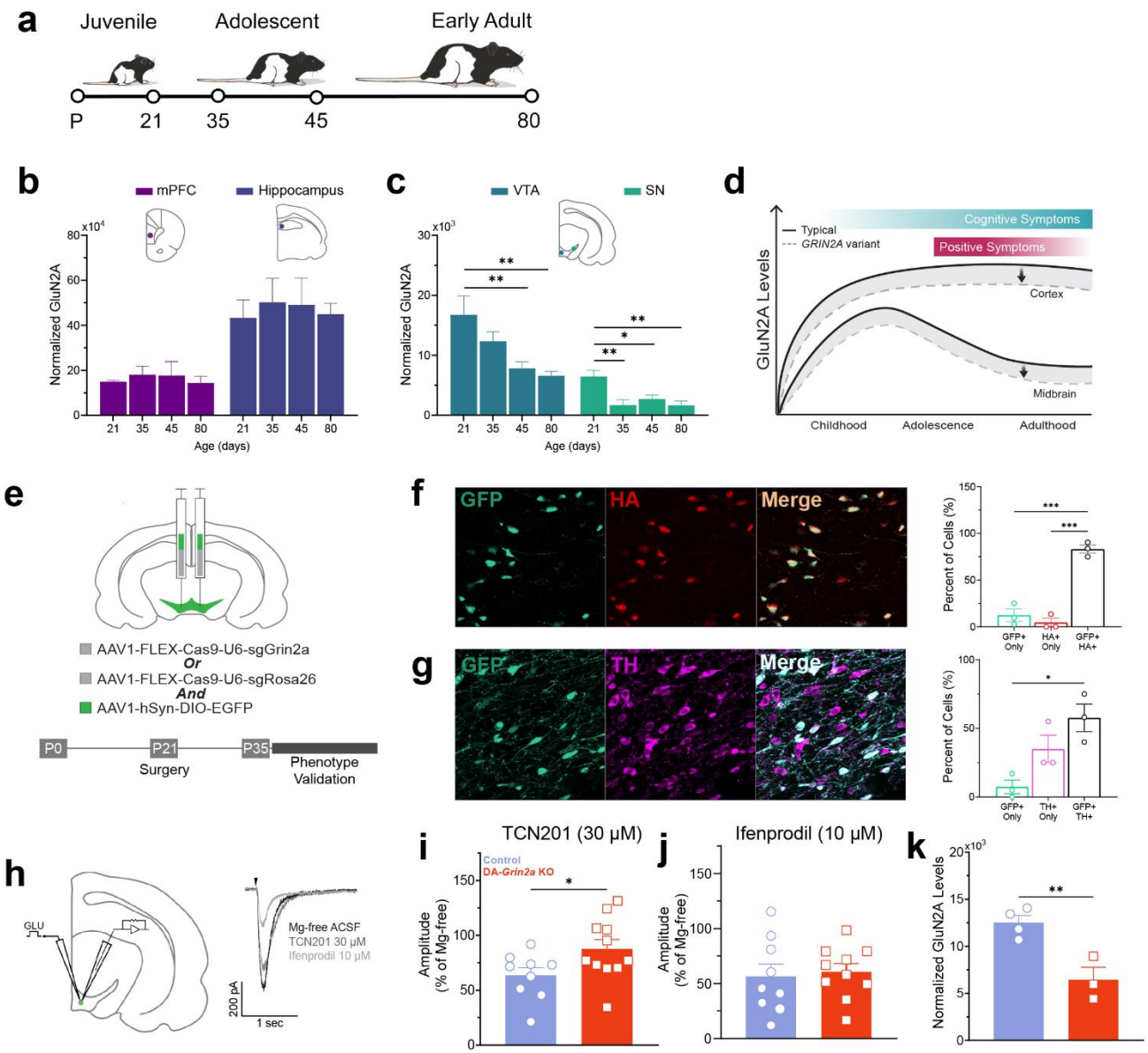

Figure 1: GluN2A loss in adolescent midbrain was augmented with virally mediated *Grin2a* loss in dopamine neurons.

a, Timeline of tissue collection ages for juvenile (P21), adolescent (P35, P45), and adult (P80) samples. **b,** Prefrontal cortex (PFC) and hippocampus showed no effect of adolescence on normalized GluN2A levels. **c,** Ventral Tegmental Area (VTA) showed significant effect of age, with reductions in normalized GluN2A at P21 vs P45 (**p*=0.0157) and vs P80 (***p*=0.0058). The substantia nigra (SN) also showed an effect of age with reductions from P21 vs P35 (***p*=0.0036), vs P45 (**p*=0.0318), and vs P80 (***p*=0.0033); (*n*=5-6 brains). Significance testing: one-way ANOVA; Dunnett post hoc. **d,** Correlation between adolescent emergence of psychosis and midbrain GluN2A loss during adolescence. **e,** Experimental design. **f,** Representative image showing GFP overlap with hemagglutinin (HA)-tagged CRISPR/Cas9 virus, quantification shows significantly more cells expressed both GFP and HA than only GFP (****p*=0.0002) or with only HA (****p*=0.0001). **g,** Representative image showing GFP overlap with dopaminergic cells, quantification shows

significantly with more cells expressed both GFP and tyrosine hydroxylase (TH) than only GFP (**p*=0.0152); (*n*=3 brains). Significance testing: one-way ANOVA; Tukey post hoc. **h,** Experimental design and example traces of slice electrophysiology experiments in adolescent brain. **i,** Quantification of peak amplitudes showed dopamine cells in DA-*Grin2a* KO brains were significantly less effected by TCN201 than controls (**p*=0.049); (control *n*=9, DA-*Grin2a* KO *n*=11 cells). **j,** Quantification of peak amplitudes showed dopamine cells in DA-*Grin2a* KO brains were similarly affected by ifenprodil as controls; (control *n*=9, DA-*Grin2a* KO *n* = 10 cells). **k,** Western blot analysis of adult brain tissue showed a significant reduction of normalized GluN2A in the VTA of DA-*Grin2a* KO animals compared to controls (***p* =0.0082); (control *n*=4, DA-*Grin2a* KO *n*=3 brains). Significance testing: unpaired t-test. Error bars denote ±SEM.

DA-Grin2a KO adolescents exhibit specific abnormalities in salience attribution in associative learning paradigms

Key characteristics of positive SCZ symptoms include delusions, hallucinations, and perceptual disorganization. The aberrant salience hypothesis of schizophrenia explains that these symptoms result from misattributed significance [32]. Over-assigning importance to irrelevant information could manifest as the abnormal beliefs and perceptions that are characteristic of emerging positive symptoms in schizophrenia [33]. Given the time constraints of the rodent adolescence period, we chose two associative learning paradigms that could be completed within two weeks and provide measures of salience attribution. These included a progressive ratio of reinforcement (PR) task and the flexible contingency learning (FCL) task.

In the PR task, the response requirement to receive a fixed reward increases over consecutive sessions (Figure 2A). This task allows for measures of (1) association learning (2) motivation through breakpoint (or highest completed ratio) and (3) measures of effort optimization and salience attribution through running response rate and post reinforcement pause length [34]. Control and DA-*Grin2a* KO animals performed similarly during the learning phases of the task: cue-action latencies, action-reward latencies, and total completed trials were not significantly different during the 7 days of training (Figure 2B-D). When preforming the progressive ratio, DA-*Grin2a* KO adolescents did not differ from controls in their breakpoint (Figure 2E) or running response rates (S2). Robust differences were, however, observed in post reinforcement pause (PRP), which is the delay between cue onset and trial initiation following a completed trial. This latency to respond typically increases as a function of an increasing response requirement [34]. Control animals displayed the expected increase of PRP as the task became more effortful, but DA-*Grin2a* KO animals did not flexibly change this response and maintained stable response latencies despite an exponential increase in action requirement (Figure 2F). Thus, while general motivational responding was normal in the DA-*Grin2a* KO animals, their abnormal

post reinforcement behavior in high effort trials suggests disrupted effort optimization and impaired ability to use feedback to optimize motivated actions.

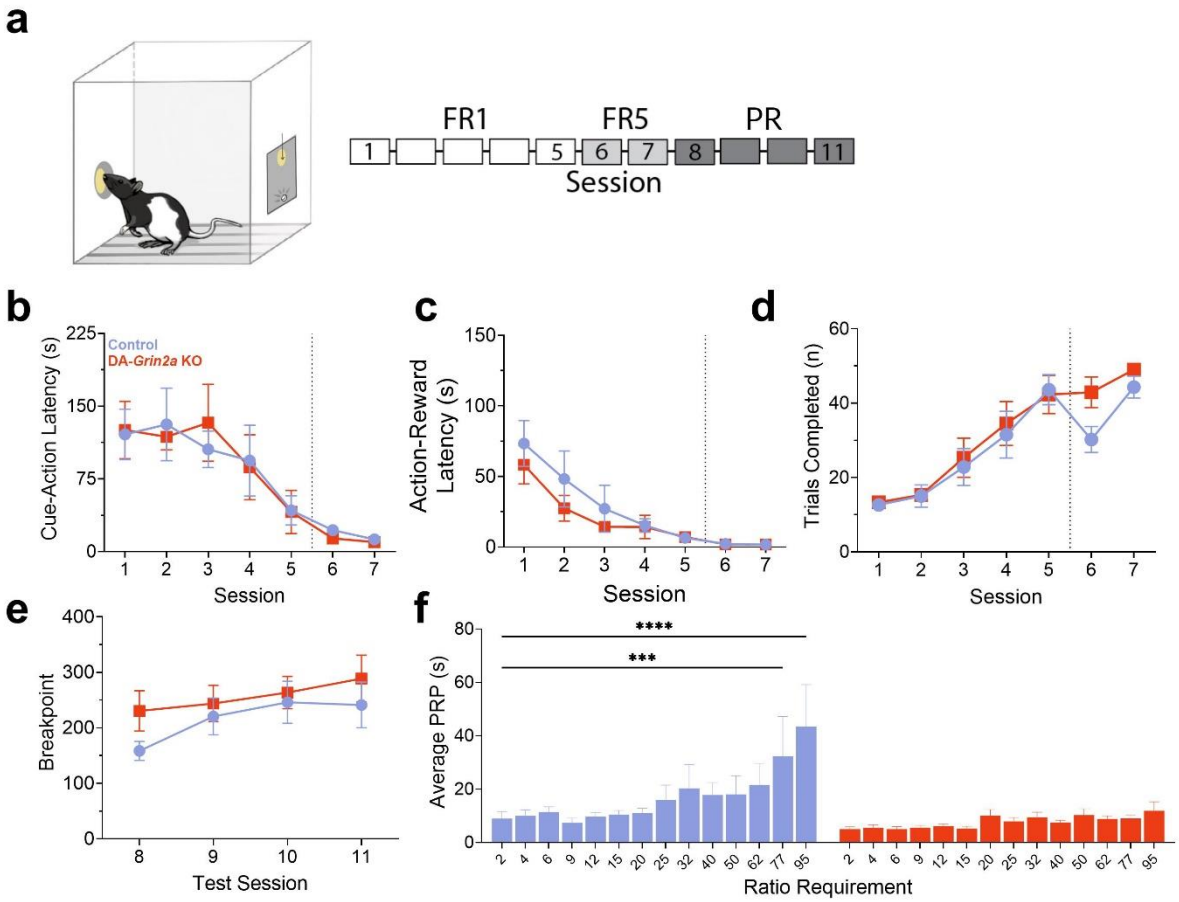

Figure 2: DA-*Grin2a* KO adolescents do not optimize effort allocation in Progressive Ratio

a, Progressive Ratio experimental design. **b,c,d,** Data collected during the FR1 and FR5 sessions show no group differences in initial operant performance. Cue-action latency (b), action-reward latency (c), and total trials completed (d) were similar between groups. **e,** DA-Grin2a KO animals showed no differences in breakpoint from controls across the four progressive ratio (PR) testing days. **f,** There was a significant interaction between treatment and ratio requirement (**p=0.0065) in average post-reinforcement pause (PRP), post hoc analysis revealed control animals increased their PRPs when the response requirement increased FR2 vs FR77 (***p=0.0005) and vs FR95 (****p<0.0001). This was not seen in the DA-Grin2a KO animals; (control n=10, DA-*Grin2a* KO n=10 rats). Significance testing: two-way ANOVA: Sidak post hoc. Error bars denote ± SEM.

Next, valence-specific behavioral flexibility was tested using a flexible contingency learning (FCL) task [35,36]. Animals were exposed to two novel conditioned stimuli (CS), which appeared in random order during the behavior session, each of which predicted the delivery of an unconditioned stimulus (US): either a reward or shock. After 5 sessions, during which associations with each CS were learned, the contingencies were switched so the CS that was initially associated with reward (referred to as CS_A) now predicted shock and the CS that previously predicted shock (referred to as CS_B) was now followed by reward delivery (Figure 3A). The key behavioral readout for this task is discrimination index (DI), which was the number of reward trough entries an animal made during each CS normalized to entries made during the inter-trial-interval (ITI). DA-*Grin2a* KO and control animals similarly learned the initial association between CS_A and reward and its subsequent association with shock (Figure 3B). Significant differences emerged in response to CS_B after the contingency switch: the initial association to the stimulus was learned similarly, but DA-*Grin2a* KO animals more rapidly developed *new* positive conditioning for CS_B compared to controls (Figure 3C).

To gain a deeper understanding of this behavioral difference, we applied computational models rooted in Pavlovian learning theory to the FCL data. We employed two distinct models: the Rescorla-Wagner model, which learns from immediate prediction errors, and the Pearce-Hall model, which focuses on stimulus associability based on prior prediction errors (Figure 3D). These models both work to explain how associations form between stimuli and outcome. They, however, differ in their ability to account for the influence of earlier stimuli presentations on information updating and related phenomena such as latent inhibition [37,38] as Pearce-Hall accounts for interactions between prior exposure and new learning. Models were fit to data collected during the initial 5 positive association learning sessions and fit both control and DA-*Grin2a* KO data with similar accuracy (Figure 3E). Data simulated using group-averaged parameter estimates successfully recapitulated our observed data (Figure 3F). These similarities were expected because with no prior learning about the reward-predicting stimulus, both models relied on similar principles of associative learning. When the models were applied to fit data from reward association learning *after* the contingency switch, we observed that the control group's behavior was better explained by Pearce-Hall whereas the DA-*Grin2a* KO animals' behavior was better explained by Rescorla-Wagner (Figure 3G). Importantly, data simulated with group-averaged parameter estimates were able to recapture the group differences we initially observed (Figure 3H). These results indicate that control animals were slower to update their response to the reward-predicting CS when that CS had previously been associated with punishment. Alternatively, DA-*Grin2a* KO animals expressed an inability to incorporate previous learning with new experiences and this led to disrupted behavioral switching when outcome contingencies changed.

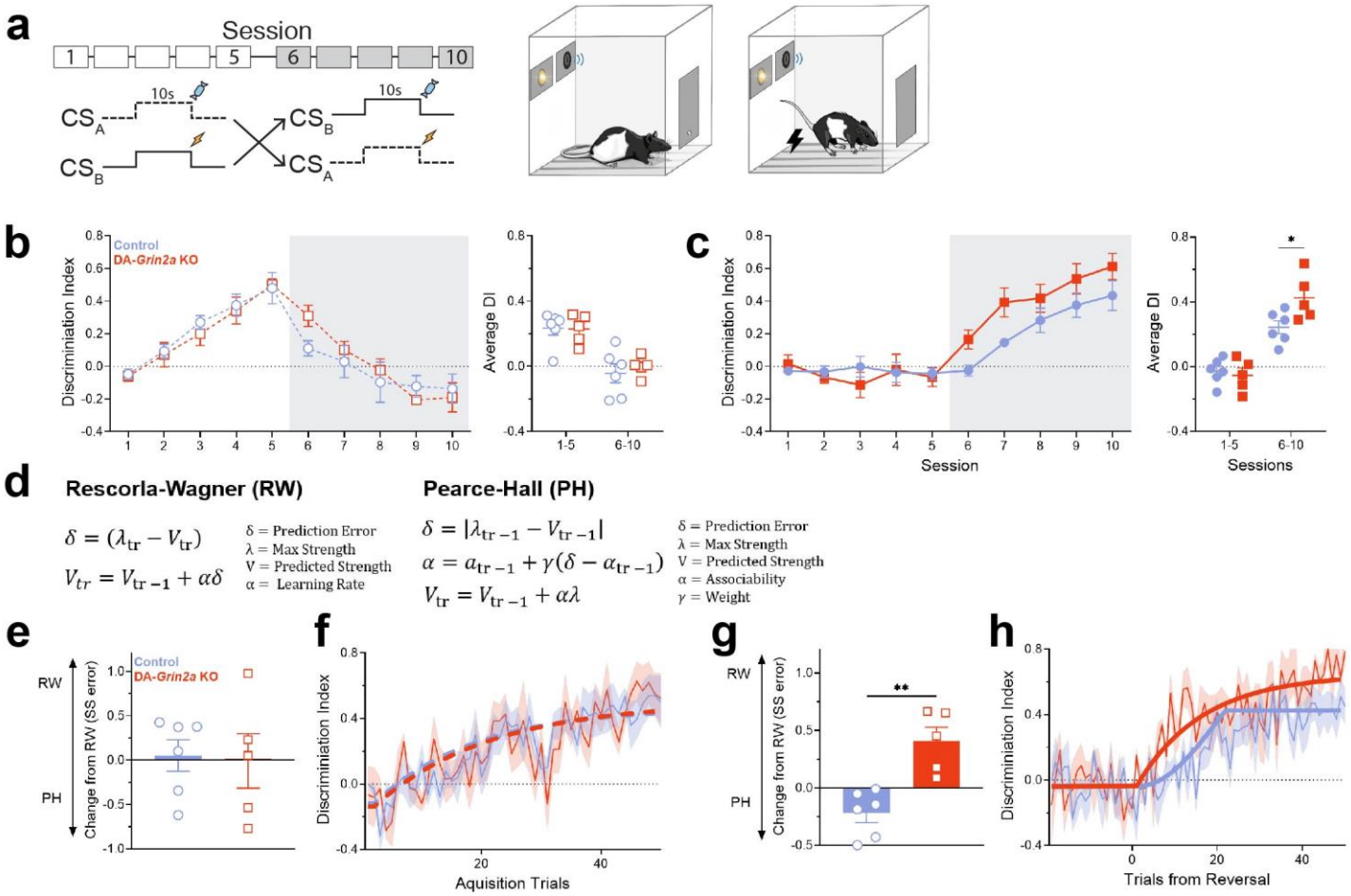

Figure 3: Computational modeling of valence specific behavioral flexibility reveals disrupted associative learning in DA-*Grin2a* KO adolescents.

a, Flexible Conditioning Learning experimental design. **b,** Discrimination index (DI) over sessions and averaged across sessions were used a behavioral readout for the FCL task. Both treatment groups responded to CS_A similarly, increasing food trough entries relative to baseline during CS presentation, then decreasing once the value of CS_A was switched on Session 6. **c,** DI over sessions and averaged across sessions in response to CS_B. There were no significant differences between treatment groups in response to CS_B over all sessions, but when DIs were pooled across initial learning (Session 1-5) and reversal (Session 6-10) DA-*Grin2a* KO animals had significantly higher DIs than controls after the contingency switch (**p*=0.0204). **d,** Summary of Pavlovian learning models applied to FCL data. **e,** Models were fit to data from the initial learning (Sessions 1-5) of the positive association (CS_A). Average and individual values (symbols) for change in model fit between Rescorla Wagner (RW) and Pearce-Hall (PH). Values <0 indicate a better fit from PH mechanisms >0 indicate a better fit from RW. These models fit the initial learning data with similar accuracy. **f,** Actual (thin lines) and predicted (bold lines) DIs for the best fit model for each group recovered no differences in behavioral trajectories over initial learning between groups. **g,** Models were fit to data from contingency reversal learning (Session 6-10) of the positive association (CS_B). Average and individual values (symbols) for change in model fit between RW and PH. RW model better fit data from DA-

Grin2a KO animals while PH better fit control data (**p=0.0016). **h,** Actual (thin lines) and predicted (thick lines) DIs for the best fit model for each group recovered differences in behavioral trajectories over learning between groups; (control n = 6, DA-*Grin2a* KO n = 5 rats). Significance testing: unpaired t-test. Error bars and shading denote ± SEM.

DA-Grin2a KO behavioral phenotype does not generalize to cognitive deficits or anxiety-related symptoms in adolescents

Finally, given the highly specific behavioral deficits observed above, we sought to determine if adolescents with the DA-*Grin2a* KO had disrupted spontaneous behaviors that may be relevant to affective and cognitive symptoms of SCZ. We conducted a battery of un-rewarded behavioral tasks aimed to assess spontaneous locomotor activity, innate anxiety, and spatial working memory. These included open field, elevated plus maze, and plus-maze to measure spontaneous alternation. In the open field, avoidance of the center portion of the maze is related to anxiety in rodents [39]. Control and DA-*Grin2a* KO rats showed no significant difference in anxiety-like behavior as they spent similar percent time in the center of the Open Field (Figure 4A). Moreover, this was not a result of an impairment in locomotor ability, as both treatment groups traveled similar distances (Figure 4B). As in the open field, avoidance of the open arms of the elevated plus maze and preference for the walled-in, closed arms can be used to ascertain anxiety-like behavior in rodents [40]. Here we further established no change in anxiety-like behavior in the DA-*Grin2a* KO adolescents as they spent similar percent time in the open and closed arms of the elevated plus maze compared to controls (Figure 4C,D). To compare spatial working memory between treatment groups, we measured spontaneous alternation in a plus maze. Because rats tend to explore novel arms as opposed to previously visited ones, impairments in working memory would emerge as reduced alternation in this task [41]. There were no significant between-group differences in spontaneous alternation in the plus maze, suggesting no effect of the DA-*Grin2a* KO on spatial working memory in adolescents (Figure 4E). This was not due to differences in overall exploration of the maze as total arm entries were also similar between control and DA-*Grin2a* KOs (Figure 4F).

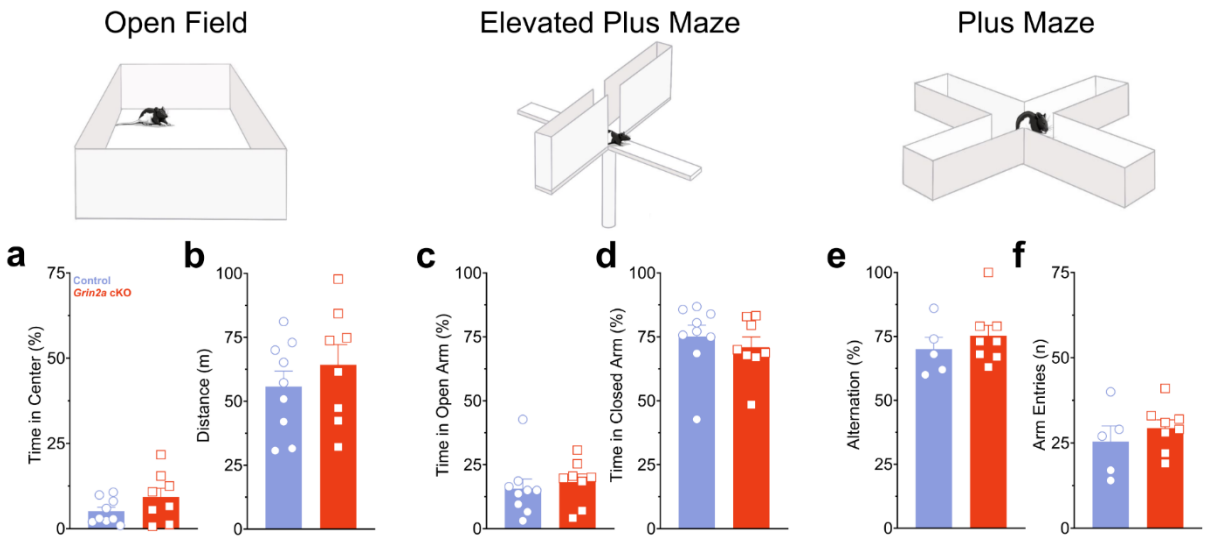

Figure 4: DA-*Grin2a* KO adolescents do not show changes in spontaneous locomotion, anxiety-like behavior or spatial working memory

a,b, DA-*Grin2a* KO animals showed no significant differences from control animals in time spent in the center of the Open Field or in general locomotor activity; (control *n*=9, DA-*Grin2a* KO *n*=8 rats. **c,d,** Control and DA-*Grin2a* KO animals showed similar percent time spent in either the open or closed arms of the Elevated Plus Maze; (control *n*=9, DA-*Grin2a* KO *n*=8 rats. **e,f**, DA-*Grin2a* KO animals had no significant differences from controls in percent alternation or total arm entries in the Plus Maze; (control *n*=5, DA-*Grin2a* KO *n*=8 rats). Significance testing: unpaired t-test. Error bars denote ± SEM.

DA-Grin2a KO disrupts dopamine release during prediction error signaling in adult animals

Disruptions in striatal dopamine neurotransmission are consistently reported in people with SCZ and in individuals at high risk to develop this disorder [26,28,29,42]. Notably, these disruptions are subtle and do not involve overt changes in dopamine related measures in postmortem or imaging studies. Instead, PET and fMRI studies have reported small but consistent disruptions in presynaptic activity [43] and in prediction error signaling in people with SCZ [44,45]. Consistent with a lack of an overt disruption of dopaminergic signaling resulting from the DA-*Grin2a* KO, we observed specific abnormalities in adolescent behavior, rather than robust changes in basal locomotion, run-time in behavioral tasks, or amphetamine-induced locomotion (Figure S3). To determine the long-term consequences of our DA-*Grin2a* KO on prediction error signaling, we measured dopamine in the nucleus accumbens core (NAc) of adult animals preforming the FCL task using fiber photometry with a fluorescent dopamine reporter ($GRAB_{DA}$) (Figure 5A-C, S4, S5) [46]. This event-rich task allowed us to assess phasic dopamine responses to novel stimuli,

their transition to predictive stimuli, as well as to expected and unexpected reward and shock delivery during learning and after shifting contingencies.

We first compared novelty responsivity between treatment groups by comparing dopamine responses to both CS_A and CS_B in early trials of Session 1—before any association learning had occurred (Figure 5D). We binned data from the first 25 presentations of either stimulus into trials of 5 to look at response to cue onset across early trials (Figure 5E). We determined the dopamine response to both CS_A and CS_B fell during trial progression similarly between treatment groups, suggesting novelty signaling was not disrupted by our manipulation (Figure 5F). Because of this novelty response, we only included the final 25 trials of each CS in subsequent analyses of Session 1 data. The same strategy was applied to Session 6 data, which was split in half to analyze separately as this was the first day of the contingency switch.

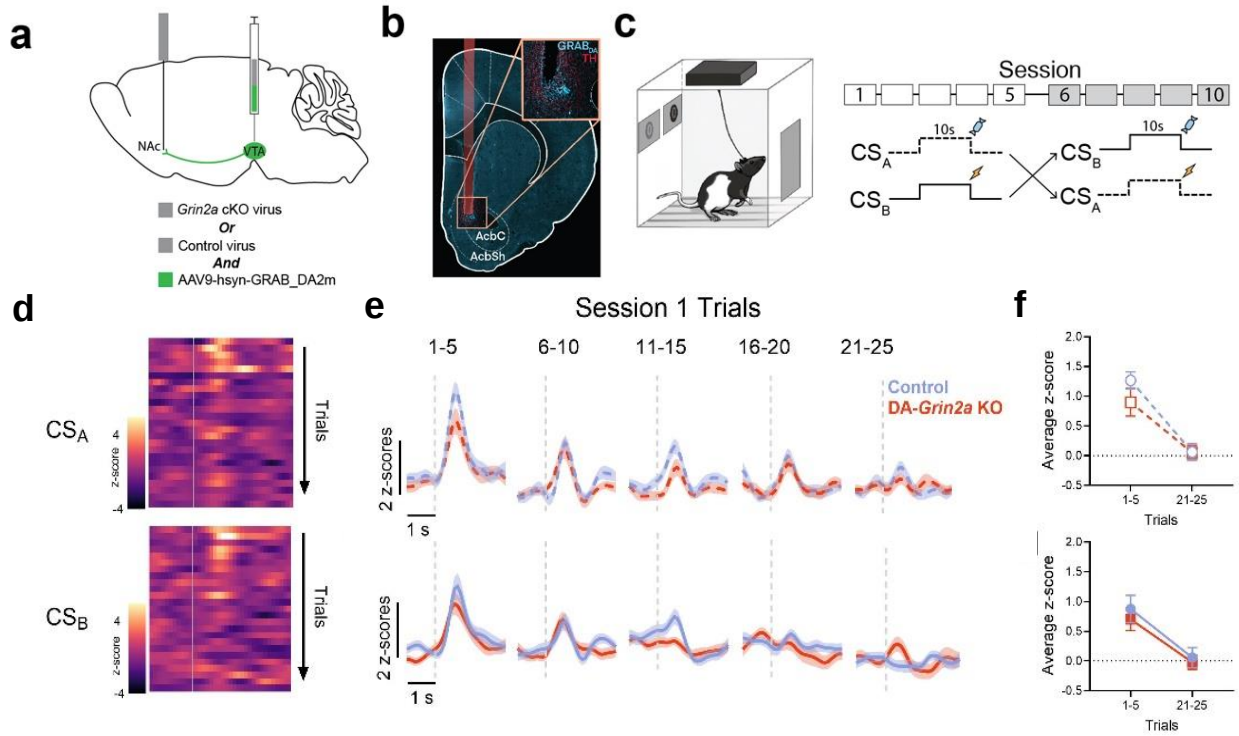

Figure 5: Dopaminergic response to novelty is conserved in adult DA-*Grin2a* KO animals

a, Virus infusion and fiber implant experiment. **b,** Example image of fiber placement into the Nucleus Accumbens core (AcbC). **c,** Fiber photometry recording during Flexible Contingency Learning task. **d**, Representative heatmaps of first 25 presentations of CS_A and CS_B during Session 1. **e,** Average fluorescent signal in first 25 presentations of either CS during Session 1, binned into 5 trial sections. **f,** Quantification of average z-score across 2 s following CS_A or CS_B onset showed reduction in response from first 5 presentations to final 25 presentations. Both control and DA-*Grin2a* KO

animals' responses fell similarly; (control *N* = 5, DA-*Grin2a* KO *N* = 6 rats). Significance testing: two-way ANOVA. Error bars and shading denote ±SEM.

To determine if there were differences in dopaminergic response to the CS and its associated US during the task, we focused our analysis to 3 periods (P1: CS onset, P2: mid-CS, and P3: US onset; Figure S6). Recordings were collected during initial association learning (Session 1 and Session 5) and following the contingency switch (Session 6 and Session 10) (Figure 6A). As the initial positive association was formed with $CS_{A,}$ we observed the expected increase in phasic dopamine response to CS_A onset in control animals by Session 5, but this effect was significantly reduced in DA-*Grin2a* KO animals (Figure 6B). When the contingency switched to a negative association, this response fell similarly between groups. This pattern was also observed when we looked at fluorescent response during mid-CS_A presentation, where again, control animals showed an elevated dopaminergic response compared to DA-*Grin2a* KO animals in Session 5 (Figure 6C). These deficits were specific to the CS, as the phasic response to the US changed similarly between both groups across sessions (Figure 6D).

The same approach was applied to fiber photometry data collected during CS_B trails (Figure 6E). As the initial negative association was formed with $CS_{B,}$ we observed a reduction in phasic dopamine response to the onset of CS_B in control animals by Session 5, but this dampened response was not observed in DA-*Grin2a* KO animals. When the contingency switched to a positive association, both groups showed increases in phasic dopamine response to CS_B onset, but control animals showed significantly higher responses to the cue than DA-*Grin2a* KO animals in Session 10 (Figure 6F). As well, throughout all sessions, controls showed average higher responses during mid-CS_B presentation (Figure 6G). Importantly, like CS_A trials, these deficits were specific to CS_B, as the phasic response to the US did not differ between groups (Figure 6H).

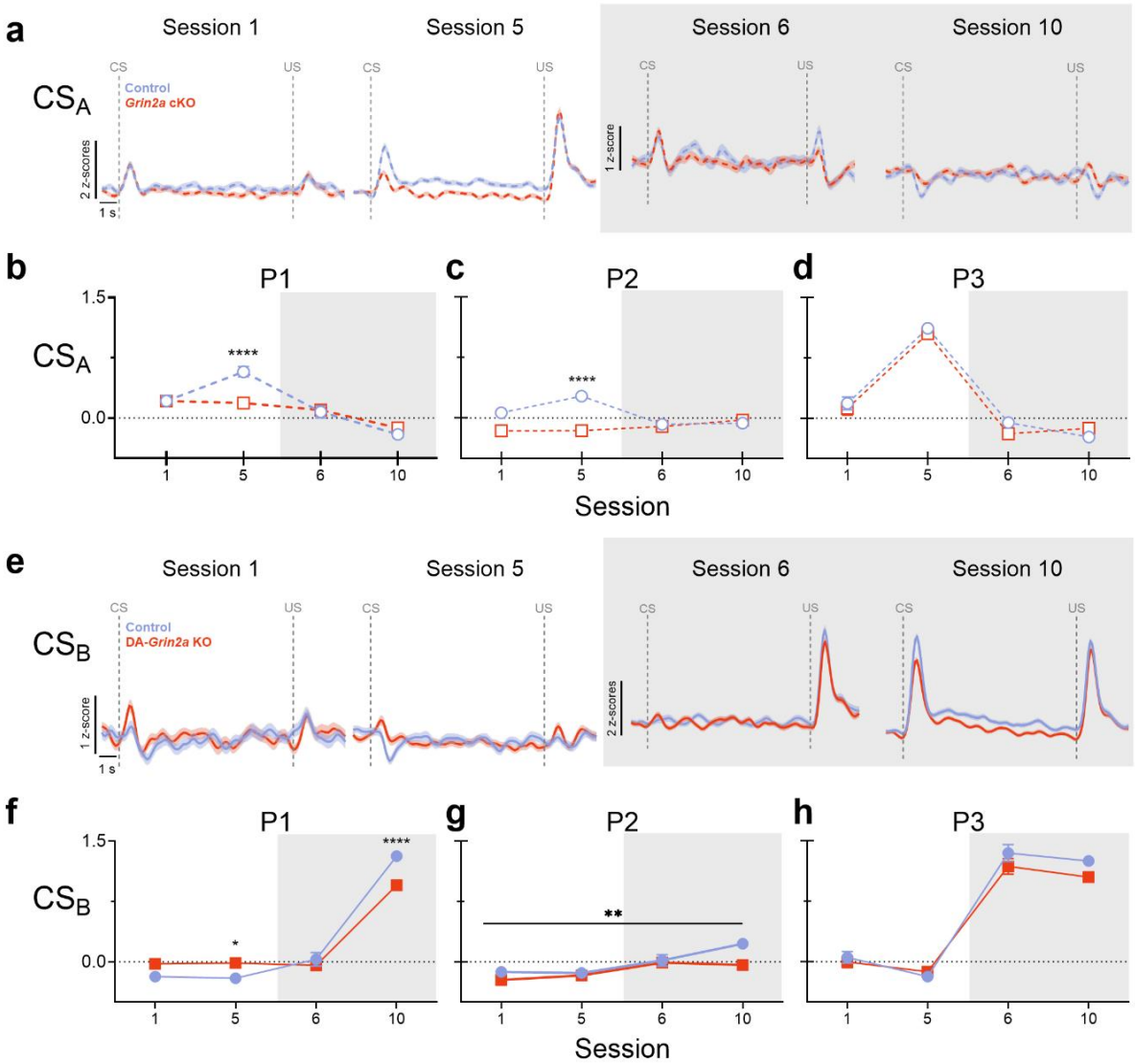

Figure 6: DA-*Grin2a* KO weakens dopaminergic response to reward-predicting cue during initial association learning in adult animals

a, Average fluorescence response during the final 25 CS_A presentations of Session 1, all 50 CS_A presentations of Session 5, final 25 presentations of Session 6, and all 50 CSA presentations of Session 10. **b,** Quantification of average z-scores during P1. Control animals showed increased average z-score during Session 5 in P1 compared to DA-*Grin2a* KO animals (****p<0.0001). **c,** Control animals had higher mid CS_A z-scores than DA-*Grin2a* KO animals (****p<0.0001). **d,** There was no difference between groups during P3. **e,** Average fluorescence response during the final 25 CS_B presentations of Session 1, all 50 CS_B presentations of Session 5, final 25 presentations of CSB in Session 6, and all 50 CSB presentations of Session 10. **f,** Quantification of average z-scores during P1. Control animals showed increased average z-score during Session 5 in P1 compared to DA-*Grin2a* KO animals (*p =0.042) and then rose to higher levels by Session 10 (****p<0.0001). **g,** Control animals had higher mid CS_B z-scores than DA-*Grin2a* KO animals (**p=0.0041). **h,** There was no

difference between groups during P3; Session1, Session 6: control n = 125 $CS_{A/B}$ trials (N = 5 rats), DA-*Grin2a* KO n = 150 $CS_{A/B}$ trials (N = 6 rats). Session 5, Session 10: control n = 250 $CS_{A/B}$ trials (N = 5 rats), DA-*Grin2a* KO n = 300 $CS_{A/B}$ trials (N = 6 rats). Significance testing: two-way ANOVA: Sidak post hoc. Error bars and shading denote ± SEM.

Finally, we analyzed Session 6—the first day the contingencies were reversed—in more detail by comparing 'Early' (first 25 trials of each CS) to 'Late' (final 25 trials of each CS) sessions. In Early CS_A trials, control animals showed heightened responses during all three periods, but these decreased by the Late trials of Session 6. This elevation in dopamine was significantly muted in the DA-*Grin2a* KO rats (Figure 7A, B). Similarly, we compared fluorescent response to CS_B, which was initially associated with shock but switched to be rewarding in Session 6 (Figure 7C). While neither treatment group showed a response to CS_B in Session 6, control animals' response to the unexpected reward was higher than DA-*Grin2a* KO animals but then normalized by Late trials (Figure 7D).

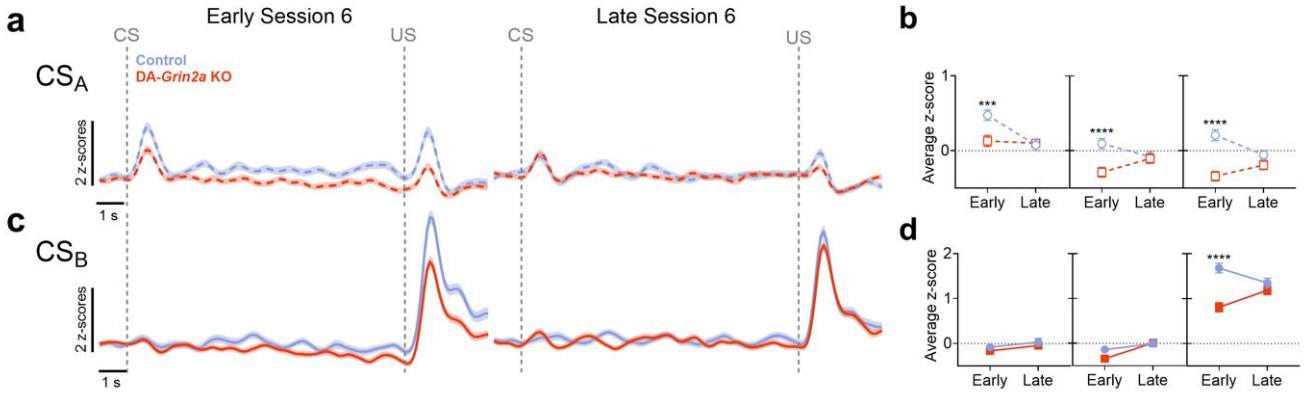

Figure 7: DA-Grin2a KO adults show abnormal dopaminergic responses when outcome is unexpected

a, Average fluorescence response during the first 25 (Early) and final 25 (Late) CS_A trials. **b,** Quantification of average z-score across 2 s time periods at CS onset (P1), mid CS (P2), and US onset (P3). Control animals had significantly higher responses than DA-*Grin2a* KOs in Early trials during P1 that fell by Late trials (left) (***p=0.0009). This difference was sustained through P2 (middle) (****p<0.0001) and P3 (right) (****p<0.0001). **c,** Average fluorescence response during the first 25 (Early) and final 25 (Late) CS_B trials. **d,** Quantification of average z-score during P1, P2, and P3. There were no differences during P1 (left) or P2 (middle). Control animals had significantly higher responses to the unexpected shock during Early trials that normalized by Late trials (****p<0.0001) (right); Early Session 6: control n =125 $CS_{A/B}$ trials (N=5 rats), DA-*Grin2a* KO n=150 $CS_{A/B}$ trials (N =6 rats). Late Session 6: control n=125 $CS_{A/B}$ trials (N=5 rats), DA-*Grin2a* KO n=150 $CS_{A/B}$ trials (N=6 rats). Significance testing: two-way ANOVA: Sidak post hoc. The data are represented as mean ± SEM.

DISCUSSION

Informed by both GWAS and exome sequencing studies [6,8,9,47], we developed a rodent model with construct and face validity that provides insight about how variants of *GRIN2A* can lead to delayed onset of psychosis and dopamine abnormalities in SCZ. Our approach was guided by the well-established clinical literature showing a relationship between dopamine neurotransmission, aberrant salience, and psychosis [26-30,32,33,42,48] which often emerge later in development than cognitive and affective symptoms. *GRIN2A* encodes the GluN2A subunit of the NMDA receptor and has a cortical developmental expression profile that corresponds with the emergence of cognitive symptoms in childhood and early adolescence. We found that—unlike cortical regions where GluN2A levels remain stable throughout adolescence—there was significant loss of GluN2A in the dopamine neuron-containing regions of the midbrain during this developmental period. This led us to reason that the *GRIN2A* variants observed in the clinical population may exacerbate this developmental decline and contribute to the emergence of psychosis. We find that a genetically driven deficit of *Grin2a* in midbrain dopamine neurons of adolescent rats is sufficient to recapitulate behaviors and dopaminergic abnormalities that are consistent with psychosis. At a fundamental level, our findings describe a novel role for GluN2A expression by dopamine neurons in prediction error signaling. These findings also provide an etiologically relevant model for latent expression of psychosis which may aid with the development of novel course alternating treatments for SCZ.

GRIN2A and schizophrenia

Genetic variants resulting in a loss of function of *GRIN2A* have been associated with schizophrenia diagnosis[6,8,9,47] , providing further credence to the long-standing theory that abnormalities in NMDA receptor function are a core component of schizophrenia pathophysiology [49,50]. These genomic findings have driven investigation into the specific role of this gene in schizophrenia pathophysiology. Global heterozygous loss of *Grin2a* in mice produces sustained phenotypes such as motor and cortical activity abnormalities and changes in expression of multiple genes relevant to schizophrenia[12 13]. These global KO studies prompted our investigation into age and cell type-specific consequences of *Grin2a* loss of function. We were specifically interested in how a *GRIN2A* loss of function may lead to latent expression of psychosis. Unlike cognitive or negative symptoms of schizophrenia, which may emerge in childhood and early adolescent, psychosis often emerges in late adolescence and early adulthood. Moreover, psychosis is associated with abnormalities in dopamine neurotransmission [25-30]. The led us to ask if selective loss of function of *Grin2a* in the dopamine neurons of adolescents is sufficient to produce phenotypes that are relevant to psychosis. We used a Cre-driven CRISPR/Cas9 virus in th::Cre male and female rats to induce a genetically driven deficit of *Grin2a* in midbrain dopamine neurons of adolescent rats. This approach was successfully implemented despite the short duration of rodent adolescence. Moreover, the animals lacked any gross

motor or learning deficits as measured by operant and maze tasks. The behavioral and dopamine release changes we observed were highly selective to constructs relevant to salience misattribution.

DA-*Grin2a* KO results in disrupted salience attribution

The core features of psychosis and related positive SCZ symptoms are delusions, hallucinations, and disorganized thoughts and perceptions. While psychosis can be difficult to model, some components of it can be studied in rodents. For example, hallucinations and delusions can result from misattributed salience [32]. Typically, our brains begin to ignore predictable sensory input to more effectively divert resources to attend to novel or consequential information. If an individual is experiencing abnormalities in perception, they attend to stimuli that would generally be ignored [33]. Here we assessed perceptual and salience attribution abnormalities using two distinct paradigms that utilized operant and classical conditioning and that could be completed within the short period of rodent adolescence. In the operant progressive ratio task, DA-*Grin2a* KO adolescents lacked the ability to suppress and adapt stimulus-driven responses. In the classical conditioning task, behavioral differences between control and DA-*Grin2a* KO animals were observed selectively during contingency reversal sessions. These behavioral data, reinforced with modeling, revealed disrupted salience attribution in DA-*Grin2a* KO animals including reduced capacity to use feedback to guide behavior by incorporating previous learning with new experiences.

DA-*Grin2a* KO results in disrupted dopamine signaling

Abnormalities in dopamine neurotransmission in people with SCZ are consistently reported. Evidence for faulty prediction error signaling in schizophrenia comes from fMRI studies showing abnormalities in regional activity during reinforcement learning. Specifically, it has been shown that midbrain and striatal activity levels in response to reward predicting stimuli are significantly lower than controls and, conversely, higher in response to neutral information [51-54]. Additionally, people with SCZ have reduced activity in the midbrain and ventral striatum when presented with an unexpected outcome while maintaining a typical level of activity in response to expected outcomes [55,56].Our data show that while approach behaviors were similar between treatment groups during initial association learning, there were disruptions in synaptic dopamine during the presentation of predictive stimuli. Even though the dopaminergic response to reward and punishment was intact in the DA-*Grin2a* KO animals, control animals developed a learned response to predictive stimuli that DA-*Grin2a* KO animals did not. This abnormal response was independent of stimulus valance, as signaling in response to the reward-predicting stimulus was reduced in DA-*Grin2a* KO animals, and their response to the punishment-predicting cue was increased. Thus, while saliency encoding was not significantly affected by the dopamine neuron-specific loss of *Grin2a*, there were disruptions value representation.

To drive learning, dopamine neurons increase activity when an unexpected event occurs [57,58]. After the contingency reversal, the robust increases in synaptic dopamine in early trials was attenuated in the DA-*Grin2a* KOs. This suggests that the DA-*Grin2a* KO impairs the ability of dopamine neurons to increase signaling when there is a difference between expected vs received outcomes. Finally, we looked at changes in dopamine signaling with learning after the contingency reversal. Our data show that during reversal sessions, both control and DA-*Grin2a* KO animals developed a phasic dopamine response to the onset of the reward-predicting cue but this was blunted in the DA-*Grin2a* KO animals. Moreover, they did not develop a dopaminergic response that persisted throughout CS_B presentation like controls and there was an overall reduction their response to reward delivery. These data suggest DA-*Grin2a* KO disrupts reward signaling updating in adult animals.

Together these data demonstrate a specific role for GluN2A-containing NMDA receptors in dopamine neurons in prediction error signaling during predictive and unexpected stimuli. These data are also consistent with clinical data of disrupted midbrain and striatal activity levels in response to reward-predicting stimuli [51-54] and when presented with an unexpected outcome [55,56]. These data provide a potential mechanism through which a genetic variant of *GRIN2A* could contribute to the deficits in prediction error encoding observed in people with SCZ.

Conclusion and Limitations

Our findings provide mechanistic insight into how variants of *GRIN2A* may lead to the latent presentation of abnormalities in dopamine dynamics in SCZ. Our aim was not to produce a full model of *GRIN2A* loss of function, but to tease apart how different cell-types and neural systems may be affected by this mutation. While in the human condition, the mutation is not confined to a single region, our approach is mechanistically informative and provides a novel potential model for designing and testing course-altering treatments for SCZ. Decades of translational studies focused on the NMDA receptor have led to the discovery of potential treatments for SCZ [49,59,60], some of which showed clinical efficacy for symptom amelioration only in younger individuals [61]. Clinical trials with these drugs may have failed in the past because they were tested in chronically ill patients with decades of antipsychotic drug treatment, which may have remodeled and changed the nature of dopamine abnormalities. In younger people with—or at high risk to develop—SCZ, these targets or newer GluN2A-selective positive allosteric modulators may provide a precise approach for preventing or altering the course of the illness.

Acknowledgments

We thank Alina P. Bogachuk for technical assistance and support with graphic design, and Dr. Selena Schattauer for assistance with viral purification. Support was also provided

from specific research grants: R01MH048404, R01MH115027, R01MH104450 and (in part) by the Intramural Research Program of the NIMH under ZIAMH002983 .

Author Contributions

M.L.K. performed protein quantification, immunohistochemistry, behavioral, and fiber photometry experiments. D.S.J. and A.J.L. performed computational analysis of behavioral data. A.T.P., J.J.L., and J. T. W. performed slice electrophysiology experiments. L.S.Z. designed and provided viruses utilized in the study. Research support to B.M. and L.S.Z. funded the work. B.M. and M.L.K. wrote the manuscript with contributions from D.S.J, A.J.L, A.T.P., J.J.L, and L.S.Z .

METHODS

Subjects

All animal procedures were approved by the Institutional Animal Care and Use Committee at Oregon Health & Science University. Long Evan's male and female rats were bred in house and maintained on a reverse 12hr light/dark cycle with ad libitum access to food and water unless otherwise stated.

Tissue collection and protein extraction

Brain levels of GluN2A were examined in animals aged P21, P35, P45, and P80. Tissue collection methods were adapted from Wager-Miller [62]. Briefly, at age of interest, brains were harvested, and flash frozen in isopentane that was pre-chilled with dry ice. Whole brains were stored in conical tubes at -80°C until dissection.

While maintaining a frozen condition, brains were sliced into 1mm sections using a pre-chilled brain matrix and razor blades. Bilateral micropunches of tissue were collected from regions of interest using a rat brain atlas as a reference [63]. To extract protein, tissue samples were homogenized in a lysis buffer containing protease and phosphatase inhibitors. Protein concentration was quantified with a Pierce BCA Protein Assay Kit (ThermoFisher). Homogenates were aliquoted and stored at -80°C until use.

Protein quantification

Automated immuno-quantification was run on a Wes instrument (Bio-Techne) according to the manufacturer's protocol [64]. Briefly, each tissue sample was diluted to a concentration of 0.3 µg/µL protein and mixed with dithiothreitol and a fluorescent molecular weight marker at a ratio of 5:1. These samples were heated to 95°C for 5 min for protein denaturation and then loaded into the allocated wells of the Wes plate. Other wells were loaded with blocking reagent, primary antibody (Rabbit-anti-NMDAR2A (Sigma Aldrich, #M264)), horseradish peroxidase (HRP)-conjugated secondary antibody, and a mix of Luminol-S and Peroxide (Bio-Techne Anti-Rabbit Detection Module, #DM-001). Size-based separation electrophoresis, immobilization, and immunodetection were automatically run using the capillary array system of the Wes. All samples were normalized to total protein as a loading control (Bio-Techne Total Protein Detection Module for Chemiluminescence, #DM-TP01). Densitometric analysis was performed using the Compass software (v5.0.1) from Bio-Techne.

Tissue dissection, micropunching, protein extraction, and Western blots were run as described above on punches collected from the VTA of virus infused animals.

Viral production

The Cre-inducible recombinant adeno-associated virus (AAV) vector constructs utilized in this study were produced and gifted by Larry Zweifel [65]. Viruses in these experiments were:

AAV1-FLEX-Cas9-U6-sgGrin2a for dopamine neuron-specific *Grin2a* knockout (DA-*Grin2a* KO) (Addgene, # 124850) which targets the first conserved exon (exon 6) across splice variants in both rat and mouse (sgRNA: 5' GAGCAGGCAACCGGCTTGCCC 3'). AAV1-FLEX-Cas9-U6-sgRosa26 was used as a control (Addgene, #159914) (sgRNA 5' CTCGATGGAAAATACTCCGAG 3'). These viruses were co-infused with AAV1-hSyn-DIO-EGFP (Addgene, #50457) at a 3:1 ratio to aid with visualization in subsequent experiments.

Stereotaxic surgeries

Juvenile rats (P21±1), were anesthetized with isoflurane and placed in a stereotaxic apparatus and body temperature was maintained using a water heating circulation pump (E-Z Systems). The scalp was incised and two bilateral craniotomies over the VTA were performed. Four 250 nL infusions at the bilateral VTA sites (AP= -4.9 mm, ML= ±0.7 mm, DV= -6.5 and -6.0 mm from dura) were delivered using a syringe pump (World Instruments) and micro infusion syringe (Hamilton) at a rate of 100 nL/min. To prevent backflow, the syringe was not removed until 5 min after infusions. The incision was then closed with surgical sutures, treated with triple antibiotic, and animals were administered 5 mg/kg carprofen subcutaneously to relieve pain and inflammation. Animals remained on heat and were administered oxygen until consciousness was regained, then returned to their home cage. There was a minimum of a two-week incubation period before experiments were run.

For fiber photometry experiments, juvenile (P21±1) animals were infused with either the control or DA-*Grin2a* KO virus mixed with AAV9-hsyn-GRAB_DA2m ($GRAB_{DA}$) (addgene, #140553) at a 1:1 ratio. These were infused bilaterally into the VTA as described above. Once animals reached adulthood (P60-70), they were implanted with a 400 µm optical fiber (Doric Lenses Inc) into the nucleus accumbens core (AP= +1.6 mm, ML= 1.5 mm, DV= -7.0 mm). Animals were given at least one week to recover from the implant surgery before behavioral training.

Immunohistochemistry

Animals were euthanized with an intraperitoneal (IP) injection of 400 mg/kg chloral hydrate and perfused via the vascular system with 0.1 M phosphate buffer solution (PBS) followed by 4% paraformaldehyde (PFA). Brains were removed and stored in 4% PFA at 4°C overnight, then transferred to a 30% sucrose solution and stored at 4°C until sectioning.

Coronal sections (35 µm) of each brain were collected using a cryostat (Lecia) and stored in 0.1 M PBS with 0.05% sodium azide. Free-floating sections were blocked and permeabilized at room temperature for 2 hrs in 0.1 M PBS, 0.25% Triton X, 10% normal donkey serum. Sections were then incubated overnight at 4˚ C with the following primary antibodies: chicken anti-TH (1:500, #76442, abcam), rabbit anti-GFP (1: 500, #290, abcam), or mouse anti-HA (1:500, MMS-101P, Biolegend). Sections were washed, then incubated in secondary antibodies (AlexaFluor-594; 488, 1:1000) for 2 hrs at room

temperature. Sections were washed again and mounted onto Super Frost+ slides. Coverslips were applied using Vectashield HardSet antifade mounting media. Fluorescence was imaged using a Ziess Axiovert 200 microscope and cell counting was done in Zen 2 software (Zeiss).

For fiber photometry experiments, sections containing the fiber tract were mounted onto Super Frost+ slides. Coverslips were applied using Vectashield HardSet antifade mounting media containing DAPI and imaged using a Ziess Axiovert 200 microscope and cell counting was done in Zen 2 software (Zeiss). To confirm fiber placement in the nucleus accumbens core, images were superimposed with a brain atlas [63] (See hit map, Supplementary Figure 2).

Slice Electrophysiology

Two to three weeks following virus infusion (P35-42), rats were anesthetized with isoflurane and decapitated. The brain was collected and deposited in artificial cerebrospinal fluid (ACSF) at 32–35°C containing (in mM): 126 NaCl, 2.5 KCl, 1.2 $MgCl_2$, 2.4 $CaCl_2$, 1.4 NaH_2PO_4, 25 $NaHCO_3$, and 11 Dextrose. The ACSF used for brain extraction, slicing and recovery also contained 2 mM kynurenic acid (Sigma) to prevent NMDA-mediated excitotoxic damage. Horizontal slices (220 µm) containing the midbrain were cut using a vibratome (Leica) in warm ACSF bubbled with 95% O_2/5% CO_2. Slices were allowed to recover in the same buffer at 30°C for at least 30 min prior to recording. Hemisected slices were transferred to the recording chamber, which was continuously perfused at 2 to 3 mL/min with bubbled ACSF at 34°C. In most experiments the recording buffer was identical to the collection buffer except it did not contain any $MgCl_2$, to allow for NMDA receptor activation by glutamate iontophoresis. In a subset of recordings, experiments were started in Mg-containing ACSF and Mg-free ACSF was perfused later. All experiments were completed within 7 h of slicing.

VTA dopamine neurons were identified by their morphology and the presence of GFP. Recordings were made using glass pipettes (1.0 – 2.5 MΩ resistance) filled with an internal solution containing (in mM): 100 K-gluconate, 20 NaCl, 1.5 $MgCl_2$, 10 HEPES (K), 2 ATP, 0.2 GTP, 10 phosphocreatine, and 10 BAPTA (4K). Recordings were made in whole-cell configuration. After break-in, cells were voltage-clamped at −55 mV and resistance and capacitance were monitored; cells with a series resistance ≥12 MΩ were discarded. The dopaminergic identity of the patched cells was further confirmed by the presence of a hyperpolarization-induced depolarizing current (I_h). Cells with an I_h < 200 pA were discarded. Another glass pipette was filled with a 1 M solution of monosodium glutamate (Sigma Aldrich). This pipette was lowered into the slice and placed in proximity to the patched cell, while a continuous backing current of +1.0 nA was applied. Glutamate was iontophoretically delivered by the application of 20 ms negative current pulses (-40.0 to -80.0 nA). Location and current intensity were adjusted to produce a stable depolarizing current in the patched cell.

Data were acquired with AxoGraph software (Berkeley, CA) and recordings were monitored with LabChart (AD instruments, Colorado Springs, CO). Current responses in Mg-free ACSF were recorded until at least 10 stable responses were obtained. For experiments where MG-free ACSF was perfused after patching this took up to 25 min. The slice was then perfused with Mg-free ACSF containing the GluN2A-specific antagonist TCN201 (30 μM). Responses to glutamate puffs were then recorded until a stable state was obtained or for a maximum of 20 minutes. The slice was then perfused with Mg-free ACSF containing 10 μM ifenprodil, a GluN2B-specific antagonist. Responses were measured until a stable state was reached, or a maximum of 20 min. Lastly, we bath applied 50 μM AP5 (Sigma Aldrich), a non-selective NMDA blocker, to confirm the identity of the measured currents. Because both TCN201 and ifenprodil do not readily wash out, each slice was only used for one attempted recording. Recordings were analyzed post-hoc using AxoGraph by averaging the last 5 stable pulses for each condition and measuring the peak amplitude of the resulting trace. Data are expressed as a fraction of the Mg-free baseline.

Operant and Pavlovian conditioning

For adolescent behavioral training experiments, operant box behavior was performed on animals aged P35-P45. Rats were mildly food restricted and habituated to operant boxes (Coulbourn Instruments) two days prior to experimentation. All behavioral tasks were run in red light and behavior recorded with Graphic State software (Coulbourn Instruments). Each animal received one of the following tasks:

Progressive ratio of reinforcement

Operant chambers contained one wall with a nose poke hole that could be illuminated and an opposing wall with a food trough where sucrose pellets were dispensed. Animals were initially trained on a fixed ratio one (FR1) schedule where one nose poke in response to a light cue resulted in the delivery of one sucrose pellet. After five days of training, animals advanced to an FR5 schedule for two days. For the final four days, animals were tested with a progressive ratio schedule, where the response ratio increased according to the formula $5e^{(0.2n)-5}$, where n = trial number. This resulted in an exponential increase in response requirement (1, 2, 4, 6, 9, 12 etc.) when rounded to the nearest whole number. Sessions were terminated if there was a 5 min cessation in responding, if a trial took longer than 45 min to complete, or after 3 hr total. Latencies to respond to the cue, to retrieve a reward, and total rewards received were calculated during FR1 and FR5 sessions. We determine the breakpoint for each animal across the four test dates. Running response rate and post reinforcement pause (PRP) lengths were determined from the average of the testing days. For trial-by-trial analyses in progressive ratio, only trials where 80% of animals completed a given ratio were analyzed.

Flexible contingency learning (FCL)

Operant chambers contained one wall with a light cue and speaker and an opposing wall with a food trough where sucrose pellets were dispensed. We utilized a modified version of a previously published task [35,36], abbreviated to better fit within the adolescent time window. Briefly, animals were presented with two conditioned stimuli (CS): a 10 sec light or tone. In a counterbalanced fashion, animals were conditioned to pair one CS with the delivery of a sucrose pellet and the other with a mild foot shock (180 ms, 0.2 mA). These unconditioned stimuli (US) immediately followed the termination of either CS. After five days of conditioning, the initial associations were reversed for Sessions 6-10. In each session, animals underwent 100 stimulus pairings (50 trials of each contingency) delivered pseudo-randomly with a 20 sec inter-trial interval (ITI). CS_A represents the cue that was initially appetitive and then became aversive, CS_B represents the cue that was initially aversive and then switched to appetitive.

Behavior was analyzed by normalizing the amount of nose pokes into the food trough during CS to baseline food trough entries during the ITI. The following equation was used to calculate this discrimination index (DI):

$$\left(\frac{\text{CS entries } - \text{last 10s ITI entries}}{\text{CS entries} + \text{last 10s ITI entries}}\right)$$

With this formula, a positive DI suggests conditioned approach, a null DI suggests no conditioning has occurred, and a negative DI suggests conditioned suppression. Average DIs across Sessions 1-5 were considered initial learning, while average DIs across Sessions 6-10 were considered contingency reversal learning.

Statistical analysis

Statistical analyses were performed in GraphPad Prism (Version 10.0.1). Unpaired t-tests were run in instances where two groups were compared. Otherwise, the data were analyzed with either a one- or two-way ANOVA with Tukey or Sidak post hoc corrections, respectively.

Computational modeling

We utilized computational models of learning to further dissect the pattern of responding in individual subjects in each group as measured by the DI during the FCL task (see above).

Models

We compared two reinforcement learning models that explain learning as a function of immediate prediction error (Rescorla-Wagner, RW) [66] or prior stimulus associability (Pearce-Hall, PH) [67]. In each model, the conditioned strength (V) of a

stimulus evolves trial-by-trial according to experience; we predicted the DI as a proxy for the conditioned strength (V) of the stimulus presented on each trial.

RW – Learning in the RW model depends on prediction error (δ). V develops for each trial according to the difference between actual (λ_n) and expected outcome (V_n) for a stimulus on a given trial (n). This prediction error is multiplied by a free parameter deemed learning rate (α, constrained between 0-1) which controls the rate of learning. This can be formulated as:

$$\delta = (\lambda_n - V_n)$$
$$V_n = V_{n-1} + \alpha\delta$$

PH - The PH model accounts for learning as a function of the associability (α) of a stimulus. We used an extended formulation of the PH model with gradual learning [68] where α is updated on a given trial from its previous level by a prediction error (δ) that tracks the absolute value of the difference between actual (λ_{n-1}) and expected outcomes (V_{n-1}) for that stimulus on the prior trial (n-1). This update to the associability of the stimulus is controlled by a free weighting parameter (γ, constrained between 0-1). The update to V is formulated as:

$$\delta = |\lambda_{n-1} - V_{n-1}|$$
$$\alpha_n = \alpha_{n-1} + \gamma(\delta - \alpha_{n-1})$$
$$V_n = V_{n-1} + \alpha\lambda$$

Model fitting

To address the high trial-by-trial response variability, we smoothed responses using a 5-trial moving average and fit each of the RW and PH models to the DI values for the pre- (Sessions 1-5) and post-reversal (Sessions 6-10) epochs for each subject. For the post-reversal epoch, initial expected value was determined for each subject by pre-reversal means (i.e. Sessions 4-5) and then shifted at reversal (Sessions 6-10) to the mean DI observed in the last session. This effectively normalized the minimum and maximum 'strength' of the cue across subjects, leaving the rate of learning controlled by α and γ for RW and PH as free parameters. Best-fitting model parameters were estimated through grid search across a range of 1000 equally spaced values and selected via a least-squares approach.

Model comparison

We compared models based on the total sum of squares (SS) for each group and selected the model parameters with the lowest total SS for each group. We also quantified the difference in sum of squares between RW and PH fits for each subject and compared groups using a two-tailed t-test.

Data simulations

We validated parameter estimates for α or γ by simulating group differences in the learning process using group averaged values for parameters from the superior model.

Maze behaviors

All maze testing was administered at P45-P55. Animals were habituated to handling and the testing environment two days preceding behavior trials. All behaviors were run in a dim, white light. On the day of testing, animals were habituated to the room for 2 hrs before trials were run. The assays were run as follows:

Elevated plus maze (EPM)

The EPM consisted of two opposing open arms and two opposing arms bordered with 48 cm walls. Animals were placed in the center of the maze and allowed to explore for 10 min and their movement tracked with PanLab SMART v3.0 software (Harvard Apparatus). Percent time spent in open and closed arms was evaluated.

Spontaneous alternation test

A four-arm, plus maze was used to assess spontaneous alternation as a measure of spatial working memory. In this task, distinct visual cues were positioned on all four walls of the behavioral testing room. Animals were placed in the center of the maze and allowed to explore for 10 min. The order of arm entries was recorded manually during the task. Percent alternation and total number of arm entries were evaluated. An alteration consisted of four distinct arm choices out of five consecutive arm entries. A 4/5 alternation score was determined by dividing the total number of alternations in overlapping quintuplets by the number of possible alternations and multiplying by 100.

Open field

Animals were placed in an opaque, square arena and allowed to explore for 20 min. Movement was tracked with PanLab SMART v3.0 software. During this time, baseline locomotion and percent time spent in center (defined as a 5 cm distance from the walls of the arena) was calculated.

Fiber photometry recording

Two days preceding fiber photometry experiments, implanted animals were mildly food restricted and habituated to handling, being attached to the recording patch cord, and to the testing environment. Animals were then run on the FCL task as previously described. Behavior was assessed by calculating the likelihood of food trough entry during the presentation of either CS_A or CS_B. Fiber photometry experiments were run using an RZ10X fiber photometry system (Tucker-Davis Technologies). The Quick-Release Interconnect (Thorlabs) was used to mate the implanted fiber optic cannula and the patch chord.

Excitation light was passed through a 400 µm patch cord from 465 and 405 nm LEDs (Doric Lenses Inc), sinusoidally modulated at 220 and 310-Hz, respectively. Signals were demodulated at 1kHz with a 6Hz low pass filter in real-time using Synapse software (Tucker-Davis Technologies). Time locked behavioral events from the operant box were recorded through the RZ10X digital input ports. Recording was performed on each day of the behavioral task.

Data analysis

Fiber photometry data were analyzed in Python 3 using the TDT Python package. Raw 465 nm ($GRAB_{DA}$) and isosbestic 405 nm data were split into trials (each trial began 10 s prior to CS onset and ended 10 s following US onset, i.e. a 30 s period). This was done to fit the $GRAB_{DA}$ signal to the isosbestic signal on a trial-by-trial basis using a least-squares linear fit (numpy polyfit function in Python). The fitted signals were then used to calculate change in fluorescence (ΔF/F) for each trial to correct for motion artifacts and photobleaching.

To assess changes in striatal dopamine around specific events (CS and US onset), peri-event z-scores were computed by comparing the ΔF/F to the 10 s baseline ΔF/F prior to CS onset, in the ITI. To quantify differences in synaptic dopamine between the treatment groups, we determined the average z-score across three, 2 s periods (P1, P2, P3). The CS onset time bin consisted of the first 2 s following the cue turning on (P1), the mid CS 2 s time bin was taken 5 s following the onset of the cue (P2), and the US onset time bin consisted of the first 2 s following the onset of the reward/shock (P3).

Statistical analyses were performed in GraphPad Prism (Version 10.0.1). Average z-scores were analyzed with a two-way ANOVA (with factors Session and Treatment) with Sidak post hoc corrections if there was a significant interaction ($p<0.05$).

REFERENCES

1. Solmi, M., Seitidis, G., Mavridis, D., Correll, C.U., Dragioti, E., Guimond, S., Tuominen, L., Dargel, A., Carvalho, A.F., Fornaro, M., et al. (2023). Incidence, prevalence, and global burden of schizophrenia - data, with critical appraisal, from the Global Burden of Disease (GBD) 2019. Mol Psychiatry. 10.1038/s41380-023-02138-4.
2. Hilker, R., Helenius, D., Fagerlund, B., Skytthe, A., Christensen, K., Werge, T.M., Nordentoft, M., and Glenthoj, B. (2018). Heritability of Schizophrenia and Schizophrenia Spectrum Based on the Nationwide Danish Twin Register. Biol Psychiatry *83*, 492-498. 10.1016/j.biopsych.2017.08.017.
3. Cannon, T.D., Kaprio, J., Lonnqvist, J., Huttunen, M., and Koskenvuo, M. (1998). The genetic epidemiology of schizophrenia in a Finnish twin cohort. A population-based modeling study. Arch Gen Psychiatry *55*, 67-74. 10.1001/archpsyc.55.1.67.
4. Sullivan, P.F., Kendler, K.S., and Neale, M.C. (2003). Schizophrenia as a complex trait: evidence from a meta-analysis of twin studies. Arch Gen Psychiatry *60*, 1187-1192. 10.1001/archpsyc.60.12.1187.
5. Cardno, A.G., Marshall, E.J., Coid, B., Macdonald, A.M., Ribchester, T.R., Davies, N.J., Venturi, P., Jones, L.A., Lewis, S.W., Sham, P.C., et al. (1999). Heritability estimates for psychotic disorders: the Maudsley twin psychosis series. Arch Gen Psychiatry *56*, 162-168. 10.1001/archpsyc.56.2.162.
6. Schizophrenia Working Group of the Psychiatric Genomics, C. (2014). Biological insights from 108 schizophrenia-associated genetic loci. Nature *511*, 421-427. 10.1038/nature13595.
7. Singh, T., Poterba, T., Curtis, D., Akil, H., Al Eissa, M., Barchas, J.D., Bass, N., Bigdeli, T.B., Breen, G., Bromet, E.J., et al. (2022). Rare coding variants in ten genes confer substantial risk for schizophrenia. Nature *604*, 509-516. 10.1038/s41586-022-04556-w.
8. Ripke, S., O'Dushlaine, C., Chambert, K., Moran, J.L., Kahler, A.K., Akterin, S., Bergen, S.E., Collins, A.L., Crowley, J.J., Fromer, M., et al. (2013). Genome-wide association analysis identifies 13 new risk loci for schizophrenia. Nat Genet *45*, 1150-1159. 10.1038/ng.2742.
9. Stefansson, H., Ophoff, R.A., Steinberg, S., Andreassen, O.A., Cichon, S., Rujescu, D., Werge, T., Pietilainen, O.P., Mors, O., Mortensen, P.B., et al. (2009). Common variants conferring risk of schizophrenia. Nature *460*, 744-747. 10.1038/nature08186.
10. Trubetskoy, V., Pardinas, A.F., Qi, T., Panagiotaropoulou, G., Awasthi, S., Bigdeli, T.B., Bryois, J., Chen, C.Y., Dennison, C.A., Hall, L.S., et al. (2022). Mapping genomic loci implicates genes and synaptic biology in schizophrenia. Nature *604*, 502-508. 10.1038/s41586-022-04434-5.
11. Hall, J., and Bray, N.J. (2022). Schizophrenia Genomics: Convergence on Synaptic Development, Adult Synaptic Plasticity, or Both? Biol Psychiatry *91*, 709-717. 10.1016/j.biopsych.2021.10.018.
12. Farsi, Z., Nicolella, A., Simmons, S.K., Aryal, S., Shepard, N., Brenner, K., Lin, S., Herzog, L., Moran, S.P., Stalnaker, K.J., et al. (2023). Brain-region-specific changes in neurons and glia and dysregulation of dopamine signaling in Grin2a mutant mice. Neuron *111*, 3378-3396 e3379. 10.1016/j.neuron.2023.08.004.
13. Herzog, L.E., Wang, L., Yu, E., Choi, S., Farsi, Z., Song, B.J., Pan, J.Q., and Sheng, M. (2023). Mouse mutants in schizophrenia risk genes GRIN2A and AKAP11 show EEG abnormalities in common with schizophrenia patients. Transl Psychiatry *13*, 92. 10.1038/s41398-023-02393-7.

14. Camp, C.R., Vlachos, A., Klockner, C., Krey, I., Banke, T.G., Shariatzadeh, N., Ruggiero, S.M., Galer, P., Park, K.L., Caccavano, A., et al. (2023). Loss of Grin2a causes a transient delay in the electrophysiological maturation of hippocampal parvalbumin interneurons. Commun Biol *6*, 952. 10.1038/s42003-023-05298-9.
15. Bagasrawala, I., Memi, F., N, V.R., and Zecevic, N. (2017). N-Methyl d-Aspartate Receptor Expression Patterns in the Human Fetal Cerebral Cortex. Cereb Cortex *27*, 5041-5053. 10.1093/cercor/bhw289.
16. Bar-Shira, O., Maor, R., and Chechik, G. (2015). Gene Expression Switching of Receptor Subunits in Human Brain Development. PLoS Comput Biol *11*, e1004559. 10.1371/journal.pcbi.1004559.
17. Maussion, G., Diallo, A.B., Gigek, C.O., Chen, E.S., Crapper, L., Theroux, J.F., Chen, G.G., Vasuta, C., and Ernst, C. (2015). Investigation of genes important in neurodevelopment disorders in adult human brain. Hum Genet *134*, 1037-1053. 10.1007/s00439-015-1584-z.
18. Monyer, H., Burnashev, N., Laurie, D.J., Sakmann, B., and Seeburg, P.H. (1994). Developmental and regional expression in the rat brain and functional properties of four NMDA receptors. Neuron *12*, 529-540. 10.1016/0896-6273(94)90210-0.
19. Wenzel, A., Scheurer, L., Kunzi, R., Fritschy, J.M., Mohler, H., and Benke, D. (1995). Distribution of NMDA receptor subunit proteins NR2A, 2B, 2C and 2D in rat brain. Neuroreport *7*, 45-48.
20. Creese, I., Burt, D.R., and Snyder, S.H. (1976). Dopamine receptor binding predicts clinical and pharmacological potencies of antischizophrenic drugs. Science *192*, 481-483. 10.1126/science.3854.
21. Snyder, S.H. (1976). The dopamine hypothesis of schizophrenia: focus on the dopamine receptor. Am J Psychiatry *133*, 197-202. 10.1176/ajp.133.2.197.
22. Matthysse, S. (1973). Antipsychotic drug actions: a clue to the neuropathology of schizophrenia? Fed Proc *32*, 200-205.
23. Seeman, P., Lee, T., Chau-Wong, M., and Wong, K. (1976). Antipsychotic drug doses and neuroleptic/dopamine receptors. Nature *261*, 717-719. 10.1038/261717a0.
24. Yun, S., Yang, B., Anair, J.D., Martin, M.M., Fleps, S.W., Pamukcu, A., Yeh, N.H., Contractor, A., Kennedy, A., and Parker, J.G. (2023). Antipsychotic drug efficacy correlates with the modulation of D1 rather than D2 receptor-expressing striatal projection neurons. Nat Neurosci *26*, 1417-1428. 10.1038/s41593-023-01390-9.
25. Angrist, B., Rotrosen, J., and Gershon, S. (1980). Responses to apomorphine, amphetamine, and neuroleptics in schizophrenic subjects. Psychopharmacology (Berl) *67*, 31-38. 10.1007/BF00427592.
26. Abi-Dargham, A., van de Giessen, E., Slifstein, M., Kegeles, L.S., and Laruelle, M. (2009). Baseline and amphetamine-stimulated dopamine activity are related in drug-naive schizophrenic subjects. Biol Psychiatry *65*, 1091-1093. 10.1016/j.biopsych.2008.12.007.
27. Abi-Dargham, A., Rodenhiser, J., Printz, D., Zea-Ponce, Y., Gil, R., Kegeles, L.S., Weiss, R., Cooper, T.B., Mann, J.J., Van Heertum, R.L., et al. (2000). Increased baseline occupancy of D2 receptors by dopamine in schizophrenia. Proc Natl Acad Sci U S A *97*, 8104-8109. 10.1073/pnas.97.14.8104.
28. Abi-Dargham, A., Gil, R., Krystal, J., Baldwin, R.M., Seibyl, J.P., Bowers, M., van Dyck, C.H., Charney, D.S., Innis, R.B., and Laruelle, M. (1998). Increased striatal dopamine transmission in schizophrenia: confirmation in a second cohort. Am J Psychiatry *155*, 761-767. 10.1176/ajp.155.6.761.
29. Laruelle, M., Abi-Dargham, A., van Dyck, C.H., Gil, R., D'Souza, C.D., Erdos, J., McCance, E., Rosenblatt, W., Fingado, C., Zoghbi, S.S., et al. (1996). Single photon emission

computerized tomography imaging of amphetamine-induced dopamine release in drug-free schizophrenic subjects. Proc Natl Acad Sci U S A *93*, 9235-9240. 10.1073/pnas.93.17.9235.

30. Egerton, A., Chaddock, C.A., Winton-Brown, T.T., Bloomfield, M.A., Bhattacharyya, S., Allen, P., McGuire, P.K., and Howes, O.D. (2013). Presynaptic striatal dopamine dysfunction in people at ultra-high risk for psychosis: findings in a second cohort. Biol Psychiatry *74*, 106-112. 10.1016/j.biopsych.2012.11.017.
31. Watanabe, M., Inoue, Y., Sakimura, K., and Mishina, M. (1992). Developmental changes in distribution of NMDA receptor channel subunit mRNAs. Neuroreport *3*, 1138-1140. 10.1097/00001756-199212000-00027.
32. Howes, O.D., and Nour, M.M. (2016). Dopamine and the aberrant salience hypothesis of schizophrenia. World Psychiatry *15*, 3-4. 10.1002/wps.20276.
33. Fletcher, P.C., and Frith, C.D. (2009). Perceiving is believing: a Bayesian approach to explaining the positive symptoms of schizophrenia. Nat Rev Neurosci *10*, 48-58. 10.1038/nrn2536.
34. Bradshaw, C.M., and Killeen, P.R. (2012). A theory of behaviour on progressive ratio schedules, with applications in behavioural pharmacology. Psychopharmacology (Berl) *222*, 549-564. 10.1007/s00213-012-2771-4.
35. Kim, Y., Wood, J., and Moghaddam, B. (2012). Coordinated activity of ventral tegmental neurons adapts to appetitive and aversive learning. PLoS One *7*, e29766. 10.1371/journal.pone.0029766.
36. Kim, Y.B., Matthews, M., and Moghaddam, B. (2010). Putative gamma-aminobutyric acid neurons in the ventral tegmental area have a similar pattern of plasticity as dopamine neurons during appetitive and aversive learning. Eur J Neurosci *32*, 1564-1572. 10.1111/j.1460-9568.2010.07371.x.
37. Lubow, R.E. (1989). Latent inhibition and conditioned attention theory (Cambridge University Press).
38. Lubow, R.E., and Moore, A.U. (1959). Latent inhibition: the effect of nonreinforced pre-exposure to the conditional stimulus. J Comp Physiol Psychol *52*, 415-419. 10.1037/h0046700.
39. Broadhurst, P.L. (1969). Psychogenetics of emotionality in the rat. Ann N Y Acad Sci *159*, 806-824. 10.1111/j.1749-6632.1969.tb12980.x.
40. Montgomery, K.C. (1955). The relation between fear induced by novel stimulation and exploratory behavior. J Comp Physiol Psychol *48*, 254-260. 10.1037/h0043788.
41. Kraeuter, A.K., Guest, P.C., and Sarnyai, Z. (2019). The Y-Maze for Assessment of Spatial Working and Reference Memory in Mice. Methods Mol Biol *1916*, 105-111. 10.1007/978-1-4939-8994-2_10.
42. Laruelle, M., and Abi-Dargham, A. (1999). Dopamine as the wind of the psychotic fire: new evidence from brain imaging studies. J Psychopharmacol *13*, 358-371. 10.1177/026988119901300405.
43. Howes, O.D., Kambeitz, J., Kim, E., Stahl, D., Slifstein, M., Abi-Dargham, A., and Kapur, S. (2012). The nature of dopamine dysfunction in schizophrenia and what this means for treatment. Arch Gen Psychiatry *69*, 776-786. 10.1001/archgenpsychiatry.2012.169.
44. Millard, S.J., Bearden, C.E., Karlsgodt, K.H., and Sharpe, M.J. (2022). The prediction-error hypothesis of schizophrenia: new data point to circuit-specific changes in dopamine activity. Neuropsychopharmacology *47*, 628-640. 10.1038/s41386-021-01188-y.

45. Katthagen, T., Kaminski, J., Heinz, A., Buchert, R., and Schlagenhauf, F. (2020). Striatal Dopamine and Reward Prediction Error Signaling in Unmedicated Schizophrenia Patients. Schizophr Bull *46*, 1535-1546. 10.1093/schbul/sbaa055.
46. Sun, F., Zeng, J., Jing, M., Zhou, J., Feng, J., Owen, S.F., Luo, Y., Li, F., Wang, H., Yamaguchi, T., et al. (2018). A Genetically Encoded Fluorescent Sensor Enables Rapid and Specific Detection of Dopamine in Flies, Fish, and Mice. Cell *174*, 481-496 e419. 10.1016/j.cell.2018.06.042.
47. Ohi, K., Shimada, T., Nitta, Y., Kihara, H., Okubo, H., Uehara, T., and Kawasaki, Y. (2016). Specific gene expression patterns of 108 schizophrenia-associated loci in cortex. Schizophr Res *174*, 35-38. 10.1016/j.schres.2016.03.032.
48. Howes, O.D., Montgomery, A.J., Asselin, M.C., Murray, R.M., Valli, I., Tabraham, P., Bramon-Bosch, E., Valmaggia, L., Johns, L., Broome, M., et al. (2009). Elevated striatal dopamine function linked to prodromal signs of schizophrenia. Arch Gen Psychiatry *66*, 13-20. 10.1001/archgenpsychiatry.2008.514.
49. Moghaddam, B., and Javitt, D. (2012). From revolution to evolution: the glutamate hypothesis of schizophrenia and its implication for treatment. Neuropsychopharmacology *37*, 4-15. 10.1038/npp.2011.181.
50. Olney, J.W., and Farber, N.B. (1995). Glutamate receptor dysfunction and schizophrenia. Arch Gen Psychiatry *52*, 998-1007. 10.1001/archpsyc.1995.03950240016004.
51. Murray, G.K., Corlett, P.R., Clark, L., Pessiglione, M., Blackwell, A.D., Honey, G., Jones, P.B., Bullmore, E.T., Robbins, T.W., and Fletcher, P.C. (2008). Substantia nigra/ventral tegmental reward prediction error disruption in psychosis. Mol Psychiatry *13*, 239, 267-276. 10.1038/sj.mp.4002058.
52. Radua, J., Schmidt, A., Borgwardt, S., Heinz, A., Schlagenhauf, F., McGuire, P., and Fusar-Poli, P. (2015). Ventral Striatal Activation During Reward Processing in Psychosis: A Neurofunctional Meta-Analysis. JAMA Psychiatry *72*, 1243-1251. 10.1001/jamapsychiatry.2015.2196.
53. Kirschner, M., Hager, O.M., Bischof, M., Hartmann, M.N., Kluge, A., Seifritz, E., Tobler, P.N., and Kaiser, S. (2016). Ventral striatal hypoactivation is associated with apathy but not diminished expression in patients with schizophrenia. J Psychiatry Neurosci *41*, 152-161. 10.1503/jpn.140383.
54. Ermakova, A.O., Knolle, F., Justicia, A., Bullmore, E.T., Jones, P.B., Robbins, T.W., Fletcher, P.C., and Murray, G.K. (2018). Abnormal reward prediction-error signalling in antipsychotic naive individuals with first-episode psychosis or clinical risk for psychosis. Neuropsychopharmacology *43*, 1691-1699. 10.1038/s41386-018-0056-2.
55. Morris, R.W., Vercammen, A., Lenroot, R., Moore, L., Langton, J.M., Short, B., Kulkarni, J., Curtis, J., O'Donnell, M., Weickert, C.S., and Weickert, T.W. (2012). Disambiguating ventral striatum fMRI-related BOLD signal during reward prediction in schizophrenia. Mol Psychiatry *17*, 235, 280-239. 10.1038/mp.2011.75.
56. Corlett, P.R., Murray, G.K., Honey, G.D., Aitken, M.R., Shanks, D.R., Robbins, T.W., Bullmore, E.T., Dickinson, A., and Fletcher, P.C. (2007). Disrupted prediction-error signal in psychosis: evidence for an associative account of delusions. Brain *130*, 2387-2400. 10.1093/brain/awm173.
57. Schultz, W., Dayan, P., and Montague, P.R. (1997). A neural substrate of prediction and reward. Science *275*, 1593-1599. 10.1126/science.275.5306.1593.
58. Schultz, W. (1998). Predictive reward signal of dopamine neurons. J Neurophysiol *80*, 1-27. 10.1152/jn.1998.80.1.1.

59. Balu, D.T., and Coyle, J.T. (2015). The NMDA receptor 'glycine modulatory site' in schizophrenia: D-serine, glycine, and beyond. Curr Opin Pharmacol *20*, 109-115. 10.1016/j.coph.2014.12.004.
60. Moghaddam, B., and Adams, B.W. (1998). Reversal of phencyclidine effects by a group II metabotropic glutamate receptor agonist in rats. Science *281*, 1349-1352. 10.1126/science.281.5381.1349.
61. Kinon, B.J., Millen, B.A., Zhang, L., and McKinzie, D.L. (2015). Exploratory analysis for a targeted patient population responsive to the metabotropic glutamate 2/3 receptor agonist pomaglumetad methionil in schizophrenia. Biol Psychiatry *78*, 754-762. 10.1016/j.biopsych.2015.03.016.
62. Wager-Miller, J., Murphy Green, M., Shafique, H., and Mackie, K. (2020). Collection of Frozen Rodent Brain Regions for Downstream Analyses. J Vis Exp. 10.3791/60474.
63. Paxinos, G., & Watson, C. (1998). A stereotaxic atlas of the rat brain. (New York: Academic).
64. Luck, C., Haitjema, C., and Heger, C. (2021). Simple Western: Bringing the Western Blot into the Twenty-First Century. Methods Mol Biol *2261*, 481-488. 10.1007/978-1-0716-1186-9_30.
65. Hunker, A.C., Soden, M.E., Krayushkina, D., Heymann, G., Awatramani, R., and Zweifel, L.S. (2020). Conditional Single Vector CRISPR/SaCas9 Viruses for Efficient Mutagenesis in the Adult Mouse Nervous System. Cell Rep *30*, 4303-4316 e4306. 10.1016/j.celrep.2020.02.092.
66. Rescorla, R.A., & Wagner, A.R. (1972). A theory of Pavlovian conditioning: Variations in the effectiveness of reinforcement and non reinforcement. In Classical condtitioning II Current theory and research, A.H. Black, ed. (Appleton-Century-Crofts).
67. Pearce, J.M., and Hall, G. (1980). A model for Pavlovian learning: variations in the effectiveness of conditioned but not of unconditioned stimuli. Psychol Rev *87*, 532-552.
68. Roesch, M.R., Esber, G.R., Li, J., Daw, N.D., and Schoenbaum, G. (2012). Surprise! Neural correlates of Pearce-Hall and Rescorla-Wagner coexist within the brain. Eur J Neurosci *35*, 1190-1200. 10.1111/j.1460-9568.2011.07986.x.